JOINT INSTITUTE FOR NUCLEAR RESEARCH, DUBNA
Report PI - 5398

OBSERVATION OF THE REACTION $\pi^- p \to e^+ e^- n$ AT 275 MeV

Yu.K. Akimov, L.S. Vertogradov, A.V. Dem'yanov,
A.V. Kuptsov, L.L. Nemenov, D.M. Khazins,
Yu.M. Chirkin, Yu.D. Prokoshkin, N.M. Agababyan,
I.A. Keropyan, G.G. Mkrtchyan, S.F. Berezhnev,
A.V. Kulikov and G.I. Smirnov

Dubna 1970

Translated at CERN by R. Luther
(Original: Russian)
Not revised by the Translation Service

(CERN Trans. 71-26)

Geneva
March 1971

1. Introduction

There are two reasons why it is interesting to investigate backward pion electro-production (BPP) in the reaction

(1)

Firstly, a study of BPP can produce data on the background photoproduction mechanism:

where γ^* is the virtual photon with a time-like 4-momentum $q(q^2 > 0)$. Secondly, by measuring the differential cross-sections of process (1) it is possible to study the electromagnetic structure of the pion and nucleon within the range of the time-like region.

BPP was first investigated by means of liquid hydrogen bubble chambers. [1,2] In these experiments slow π^- mesons which had stopped in the liquid hydrogen formed mesonic atoms. The majority of reaction (1) events corresponded to the small momenta transmitted ($\bar{q}^2 \approx 0.1f^{-2}$, $q^2_{max} = 0.5f^{-2}$) and therefore the hadrons' electromagnetic form factors had little effect on the probability of the process and distribution in terms of the kinematically independent variable. In defining the deviation from probabilities which correspond to structureless particles by the term a^2q^2, Kobrak obtained[2] the following value for the parameter a^2: $a^2 = (0.1 \pm 0.2)\, m_\pi^{-2}$ where m_π is the pion's mass.

A reasonable way to observe and measure the effects of hadron structure is to study reaction (1) using large pulses. The work carried out on the liquid hydrogen bubble chamber[3] included an estimate of the BPP cross-section using π^- mesons with a kinetic energy of 340 MeV. For events with $q^2 > 0{,}5f^{-2}$ the cross-section proved to be less than $6.10^{-30}cm^2$ with 95% probability, thus

indicating that it was impossible to study process (1) using chamber techniques.

In further BPP experiments performed at high energies [4] ($E_\pi > 3$GeV), the first data were obtained on the pion's form factor at $q^2 > 8f^{-2}$. This momentum range is now being investigated with a good degree of accuracy in colliding-beam experiments[5]. There is no information on pion structure at low q^2 values, except for an estimate of the electromagnetic radius[6]: $r_\pi < 1{,}9f$ with 90% confidence ($\bar{q}^{-2} \approx 0.3f^{-2}$).

The nucleon's form factor at $q^2 > 0$ has not been studied. Moreover, in future colliding beam experiments the range $0 < q^2 < 4M^2$ (M is the nucleon's mass)is not kinematically attainable. Therefore, reaction (1) is virtually the sole possible source of experimental data on nucleon structure in this momentum range. The same can be said for data on pion structure at $0 < q^2 < 4m_\pi^2$.

The theoretical examination of BPP [7,8] for mesons with kinetic energies of up to 350-400 MeV indicates that it is possible to determine form factors both for the pion and nucleon at $q^2 < 5f^{-2}$.

The aim of this paper was to observe and investigate reaction (1) for π^- mesons of 275 MeV. The experiment was performed on the synchrocyclotron in the Laboratory for Nuclear Problems at JINR.

2. Experimental Set-up

There are considerable experimental difficulties involved in the observation of reaction (1) at relatively high q^2 values. They are due to the small cross-section for this reaction ($d^2\sigma/d\Omega_1\, d\Omega_2 \approx 10^{-33}$ cm^2/sterad^2 at 275 MeV*, Ω_1 and Ω_2 are the solid angles for recording the electron and positron) and to the

---

* This estimate was obtained by multiplying the cross-section for backward pion photoproduction by the photon's internal conversion coefficient and the photon propagator.

high background level produced by the intensive nuclear interaction processes which occur between pions and protons at the same time as reaction (1). Thus, the elastic scattering cross-section

$$\pi^- + p \to \pi^- + p \qquad (2)$$

is $d\sigma/d\Omega \approx 10^{-27}$ cm^2/sterad. To suppress the recording of this process, a design (fig. 1) was chosen which prevented pions and protons from passing simultaneously through the detectors recording the electron and positron in reaction (1) (θ_1, $\theta_2 \approx 90°$).

The cross-section of the background process

$$\pi^- + p \to n + \pi^+ + \pi^- \qquad (3)$$

exceeds the cross-section of reaction (1) by three orders of magnitude. With this type of geometry, the energy of the pions incident on the device was low. By using Čerenkov counters, the probability of recording pairs of pions (3) was suppressed $\approx 10^5$ times.

The pion charge exchange reaction

$$\pi^- + p \to \pi^0 + n, \quad \pi^0 \to 2\gamma \qquad (4)$$

can also imitate process (1) when γ quanta from the decay of π^0 mesons are converted into electron-positron pairs in the surrounding matter or when inner conversion takes place. The cross-section for charge-exchange (4) is : $\sigma_t = 20$ mb. In our case the recording efficiency for this reaction did not exceed 10^{-9} and could be still further reduced by introducing particle discrimination in terms of the energy released in the Čerenkov spectrometers.

The total cross-sections of the other background processes

$$\pi^- + p \to \pi^- + \gamma + p \; ; \qquad (5)$$

$$\rightarrow \pi^- + \pi^0 + p\,, \quad \pi^0 \rightarrow 2\gamma; \tag{6}$$

$$\rightarrow n^0 + \pi^0 + n\,, \quad 2\pi^0 \rightarrow 4\gamma \tag{7}$$

equal 0,16; 0,1; and 0,4 mb. respectively. The products of these reactions can be recorded by the device when conversion of the γ quanta occurs. These processes differ from reaction (1) in that e^+e^- pairs pass through the side telescopes.

Finally, there are the interaction processes with protons of the muons and electrons which are present in the pion beam in the form of contamination.

The probability of recording these processes is extremely small ($d^2\sigma/d\Omega_1 d\Omega_2 < 10^{-36} cm^2/sterad^2$). When muons and electrons are scattered by electrons, collision kinematics also prevent both scattered particles from hitting the electron detectors.

3. The Experimental Device

Reaction (1) was examined in the synchrocyclotron's meson beam[9]. The pion's kinetic energy was determined from its path through copper and was 275 MeV with a spread of $\pm$ 15 MeV. The intensity of the beam incident on the target was 5.10^5 sec.$^{-1}$. The pion fraction in the beam was determined from elastic $\pi^- p$ scattering and was $(79\pm4)\%$. μ^- mesons were the main contamination in the beam; the electron fraction did not exceed a few per cent.

When the beam reached the target, it was separated out by scintillation counters C_1 - C_3 and by counter $\bar{C}_4$ with a central cavity (fig. 1). A veto counter $\bar{C}_5$ was placed behind the target. The electrons and positrons produced in reaction (1) were recorded by two telescopes which were used to measure the escape angles and energies of the particles. Each of the telescopes comprised a scintillation counter (C_6 and C_7), a threshold water Čerenkov

counter ($\check{C}_1$ and $\check{C}_2$) and a total absorption Čerenkov spectrometer connected in coincidence, and also a spark chamber (SC_1 and SC_2).

Each telescope recorded particles in the angular range Θ_1, $\Theta_2 = 90° \pm 20°$. The effective solid angle for the side telescopes calculated by the Monte-Carlo method, was Ω_1, $\Omega_2 = (0{,}186 \pm 0{,}007)$ster.^{2}.

The scintillation counters C_1 C_2 and C_3 measured 100 x 100 x 10 mm^3, $\bar{C}_5$ - 200 x 200 x 10 mm^3, C_6 and C_7 - 280 x 200 x 10 mm^3, C_4 - 200 x 200 x 10 mm^3 with an aperture of 100 mm diameter. FEU - 30 photomultipliers were used in the counters.

The threshold Čerenkov counters $\check{C}_1$ and $\check{C}_2$ were used to suppress the background of low-energy pions. Distilled water was used as a radiator. In order to shift the Čerenkov radiation spectrum into the sensitivity range of the FEU-30 photocathode amino-G-acid was dissolved in water in an 80 mg./litre concentration[10]. The radiator for these counters was 300 mm in diameter and 44 mm thick. Fig. 2 shows the measured dependence of a Čerenkov counter's efficiency on the velocity of the particles passing through at a discriminating threshold corresponding to 95% electron recording efficiency. The Čerenkov counter with a spectrum shifter has no directional radiation and can therefore be used in beams with large angular spread.

The total absorption Čerenkov counters were used to measure electron and positron energies and to suppress background. The radiator of spectrometer $\check{C}_3$ consists of the frustum of a cone made from LF-5 glass, the base diameters of which are 320 and 400 mm. The height of the cone is 150 mm (4,2 radiation lengths). The radiator for spectrometer $\check{C}_4$ is made from TF-1 glass and is 350 mm in diameter and 300 mm thick (12,6 radiation lengths). Each of the radiators is scanned by three FEU-65 photomultipliers whose photocathodes measure 150 mm in diameter. The photomultipliers are shielded from the $\approx$ 5 oerst. magnetic field by two

steel (St.3) screens, each 5 mm thick.

The spectrometers' pulse-height stability was periodically checked by means of light diodes[11]. Instability during the 6 months of operation on the accelerator did not exceed $\pm 4\%$. The spectrometers were calibrated on the electrons present in the meson beam[12]. The results of the calibrations are given in fig. 3.

The pulse-height spectra of counters C_6 and C_7 and the efficiency of the side telescopes were also measured in the electron beam.

The spark chambers were used to identify interactions containing two charged particles in a final state and to provide a spatial picture of the events recorded. Each spark chamber has two 22 mm gaps. The aluminium electrodes are 1 mm thick. The effective area of the chambers is 260 x 260 mm^2. The chambers are filled with neon and operate in the track mode up to angles of $\approx 30°$ with 98% efficiency. High-voltage pulses of 24 kV amplitude are shaped by a two-stage Arkad'ev-Marks generator. The total delay for a high-voltage pulse was 0,8 microsec.

The efficiency of the spark chambers reaches its maximum value at a high-voltage pulse height of $\approx$ 16 kV. The chambers' memory time for a 40 V clearing field is 2 microsec. The discharge capacity was fixed so that the track width equalled $\approx$ 1,5 mm. Under these conditions, tracks could be reproduced by the spark chambers with more than 0,5° accuracy, **and a high recording efficiency was ensured.**

The horizontal and vertical projections of both spark chambers were photographed by one camera using a system of mirrors. After the spark chambers had been filled, their characteristics remained virtually the same throughout the year.

The effective volume of the liquid hydrogen target comprises a cylinder with a diameter of 120 mm. and an effective length of 221 mm. The total thickness of the stainless steel walls is 0,6 mm (0,03 radiation lengths).

The electronic system includes 4 coincidence circuits: $СС_1(С_1 \cdot С_2 \cdot С_3 \cdot \bar{С}_4 \cdot \bar{С}_5)$, $СС_2$ $(С_6 \cdot \check{С}_1 \cdot \check{С}_3)$, $СС_3$ $(С_7 \cdot \check{С}_2 \cdot \check{С}_4)$ and $СС_4$ $(СС_1 \cdot СС_2 \cdot СС_3)$, which select time-correlated events. The resolving time τ is 5,5 nanosec. for the $СС_1$ circuit and 20 nanosec for the others. The thresholds of the discriminators in the spectrometer circuits were fixed at a level corresponding to an electron energy of 20 MeV.

The trigger-pulse was produced by the electronic circuit if the total energy release in the spectrometers exceeded 120 MeV. The trigger-pulse passed through a blocking circuit with a 0,3 sec dead time and triggered the 5-beam oscilloscope sweep, the gating circuits, the pulse-height analyzers, the spark chamber generators and the two cameras.

The pulses from all the detectors were fed to the 5-beam oscilloscope[14] whose sweep rate was 25 nanosec./cm. The oscilloscope screen was photographed together with the readings on the pulse-height analyzers which in turn were supplied with signals from the spectrometers. The time resolution τ for the oscillograms is 1,2 nanosec. for the scintillation counters, 3 nanosec. for the spectrometers and 4,5 nanosec. for the Čerenkov counters. The position of pulses in the oscilloscope's sweeps relative to the pulse from the $С_3$ reference counter within the limits of error ($\approx 0,2\ \tau$) was stable throughout the 100 hours. The combination of low time resolution for the coincidence circuits ($\tau \approx 20$ nanosec.) with the high resolution provided by the oscilloscope ($\tau \approx 1,2$ nanosec.) enabled a close study to be made of the time distribution of background events when the data were processed.

4. Measurements

During the main measurements with the monitor telescope ($C_1 \cdot C_2 \cdot C_3$), $3{,}32 \cdot 10^{11}$ particles were passed through, including $(1{,}78 \pm 0{,}11) \cdot 10^{11}$ pions which traversed the hydrogen target. The thresholds of the detectors were set so that the average trigger rate was ≈ 3 min.$^{-1}$. There was virtually no loss in recording efficiency and it was possible to operate the apparatus under continuous control. Measurements were also made using an empty target and in this case the total number of particles through the monitor telescope totalled $0{,}45 \cdot 10^{11}$.

During the measurements, the apparatus was calibrated periodically (every 8 hours) using elastically scattered pions. The oscillograms were used firstly to fix the temporary position of the pulses from all the detectors in relation to the pulse from the reference counter C_3, secondly to determine the variations in time distributions, thirdly to establish the pulse-height distributions of the scintillation and Čerenkov counters, and fourthly to check the time stability of these parameters. The efficiency of the spark chambers and the probability of random track overlapping were determined from the spark chamber frames obtained during the calibrations.

5. Processing of the Results

The measurements produced 52,000 pictures with the target full and 5,000 pictures with the target empty. During the examination of the spark chamber frames, events were selected which contained only one track in each chamber. These events were measured on the semi-automatic PUOS-50 devices. Then, using a geometry reconstruction program, the probability of two particles escaping from one point on the target was determined. For this purpose, the following value was calculated for each event

$$\chi^2_{\text{ор}} = \frac{d^2}{\Delta r_1^2 + \Delta r_2^2},$$

where d is the minimum distance between the track extensions within the target and Δ_{ri} is the RMS displacement of a track positioned close to the minimum distance between tracks. The value Δ_{ri} is conditioned by multiple scattering and by errors in the determination of track angles in the spark chambers. The multiple scattering contribution was calculated on the assumption that the tracks belonged to electrons with energies determined from the readings on the Čerenkov spectrometers. The distribution of the X_{sp}^2 value for reaction (1) events should correspond to the X^2 distribution with two degrees of freedom. Events were rejected if $X_{sp}^2 > 16$ (probability $P(X_{sp}^2 = 16) = 0{,}03$). Events were also rejected if their point of impact on the spectrometer was less than 30 mm from the edge of the instrument.

In view of the large background of charged particles passing through both side telescopes and not connected with the interaction of beam particles with the target, only those events were chosen for which the angle between the tracks θ_{12} did not exceed 165°.

To suppress the background of low-energy particles, only events with an energy release in the spectrometers of E_1, $E_2 >$ 40 MeV and $(E_1 + E_2) >$ 140 MeV were selected.

For the remaining events, the time and amplitude characteristics of pulses from all the detectors were measured and events were rejected if the deviation from the values obtained during the calibrations exceeded 3γ and also if the pulse-height in one of the C_5, C_6 counters was over 3 times greater than the most probable value.

Thus 125 candidate events for reaction (1) were obtained with the full target, and 2 events with the empty target. The time distributions of the candidates (fig. 4) correspond well with the calibrated measurements.

Taking into account the selection criteria listed above, the recording efficiency for reaction (1) events is $(58\pm3)\%$. Efficiency losses are mainly determined by the introduction of criterion $\theta_{12} < 165^\circ$ (20%), by the inefficiency of the spark chambers (13%) and of the side telescopes (8%). The efficiency value was determined from the calibrated measurements and by simulating the reaction using the Monte-Carlo method with an allowance for the detectors' resolution. The figure for the overall loss in efficiency does not include losses which occur when the criterion E_1, $E_2 > 40$ MeV is introduced: these range from 20% to 40% depending on the assumptions made concerning the dynamics of the process.

A comparison of the results obtained from the measurements with the empty and full targets shows that the 125 candidates include 15 ± 10 background events which are not related to the hydrogen. An analysis of events selected in time intervals exceeding $\pm10\sigma$ shows that the number of random coincidences for the full and empty targets, produced by the total beam used with the full target, is the same and equals approximately 4 events. Thus, the majority of the 125 candidates (110 ± 10) have been produced in hydrogen.

An analysis of the events selected showed that they included background events characterized by large pulse-height values in the side scintillation counters C_6 and C_7, corresponding to the simultaneous advent of more than one particle with minimum ionization. This background seems to result from reactions (5)-(7) with an emission of γ quanta which are converted in the target and counters. Estimates show that Bremsstrahlung from π-meson-proton scattering is the main contributor to the background (5).

In addition to selecting reaction (1) events from the candidate events according to the ionization losses, it was also specified that the missing mass, determined from the given event's parameters, should equal the neutron's mass. Therefore, the

following functional was calculated for each event

$$U = \sum_{i=1}^{7} \frac{(p_i - \tilde{p}_i)^2}{\sigma_i^2},$$

where p_i represents the event's parameters (pion momentum, electron energies and angles of emission), σ_i is the measurement errors and $\tilde{\tilde{p}}_i$ is the set of corresponding parameters which satisfy the requirement that the missing mass should equal the mass of the neutron. A set of $\tilde{\tilde{p}}_i$ parameters was chosen which corresponded to the minimum value of function U. Then the X^2_{sp} value was recalculated and, to assess the effects of multiple scattering, the electron energy values obtained by minimizing the U functional were used (this corresponds with the assumption that the event belongs to reaction (1)).

By making use of the candidates' distribution according to the value $W^2 = X^2_{kin} + X^2_{sp}$, where $X^2_{kin} \equiv \min U$, it is possible to isolate the background events. As the W^2 distribution for reaction (1) events should correspond to the X^2 law with three degrees of freedom, events with large W^2 values (the criterion $W^2 > 14$ was used) are clearly background events.

These events provide information on the distribution of ionization losses in side scintillation counters when one of the telescopes records a γ quantum. In particular it is possible to determine the probability ρ of a background event, to have one of the pulse-heights (A_6 or A_7) $> A_0$. A similar probability for reaction (1) events was determined when counters C_6 and C_7 were calibrated using electrons.

It is then possible to determine the number n of those events present in any sample of N candidates which include R events satisfying the condition (A_6 or A_7) $> A_0$, from the obvious relationship

$$R = \alpha n + \rho (N-n). \qquad (2)$$

To determine the total number n_o of reaction (1) events, candidates for which $W^2 < W_o^2 = 10$ when parameter $A_o = 1{,}6A_{prob.}$ were selected. It was found that the number of reaction (1) events equals $n_o = 57 \pm 14$. The n_o value was calculated with an allowance for losses in efficiency when the criterion $W^2 < W_o^2$ was introduced. The ambiguities of the α and ρ values and the statistical errors were taken into account when calculating the error in n_o. The n_o values obtained for various W_o^2 and A_o values are given in the table which shows that the result within the limits of error does not depend on the selection of W_o^2 and A_o values.

W_o^2	$A_o / A_{prob.}$	1,3	1,6	1,9
6			58 ± 15	
10		63 ± 21	57 ± 14	54 ± 15
14			60 ± 15	

By means of relationship (2), the distributions of reaction (1) and background events in terms of the value $W^2 = X_{kin}^2 + X_{sp}^2$ (fig. 5) were obtained from the distributions of the candidate events in terms of the same value (fig. 5). In addition, values were obtained for the distributions of reaction (1) events in terms of the total energy of electrons and positrons, in terms of the angle between them in the laboratory coordinate system θ_{12} and in terms of the effective mass of the e^+e^- pair. These distributions are shown in fig. 7. The solid curves represent the result of simulating reaction (1) in a statistical model.

Taking into account the event background with an empty target and also random coincidences, the number of reaction (1) events recorded is 55 ± 14.

Using this value, the cross-section of reaction (1) can be calculated:

$$\Delta\sigma = \int_{\Omega_1\Omega_2} \frac{d^2\sigma}{d\Omega_1 d\Omega_2} d\Omega_1 d\Omega_2 = (0{,}45 \pm 0{,}12)\cdot 10^{-33} \text{ см}^2. \qquad (8)$$

This value corresponds to that part of reaction (1) which is separated out by our device under the additional criteria E_1, $E_2 > 40$ MeV and $\Theta_{12} < 165°$.

Hence the differential cross-section of reaction (1) was calculated for electrons of energy E_1, $E_2 > 40$ MeV emitted in the angular range $70° \leq \Theta_1, \Theta_2 \leq 110°$.

$$\frac{d^2\sigma}{d\Omega_1 d\Omega_2} \approx \frac{\Delta\sigma}{\xi\Omega_1\Omega_2} = (3{,}0 \pm 0{,}8)\cdot 10^{-33} \text{ см}^2/\text{стер}^2, \qquad (9)$$

where ξ is the factor which allows for losses in reaction (1) events when the criterion $\theta_{12} < 165°$ is introduced. The ξ value, calculated by the Monte-Carlo method, does not depend on the type of theoretical model and equals 0,80.

6. Conclusion

In this paper, backward pion electroproduction (1) was observed in the "intermediate" momentum range $1f^{-2} \lessapprox q^2 < 3f^{-2}$ and its differential cross-section was measured. The data obtained show that it is possible to isolate this low-intensity reaction reliably and to increase considerably the accuracy of the cross-section measurements.

The authors wish to thank L.I. Lapidus and B.M. Pontekorvo for their unfailing interest in the paper, V.I. Petrukhin and A.I. Shchetkovskij for helping to set up the apparatus, A.A. Tyapkin for his comments, V.A. Smirnov for his part in the assembly of the experimental device, and also N.A. Vladimirova, S.G. Plastinina, V.F. Churkina and A.G. Fedunova for their considerable assistance with the processing of the experimental material.

Bibliography

1. N.P. Samios. Phys. Rev., 121, 275 (1961).

2. H. Kobrak. Nuovo Cimento, 20, 115 (1961).

3. T.D. Blokhintseva, V.G. Grebinnik, V.A. Zhukov, A.V. Kravtsov, G. Libman, L.L. Nemenov, G.I. Selinavov, Yuan'Zhyn-Fan. Ya. F.(Yadernaya Fizika) (Nuclear Physics) 3, 779 (1966)

4. S.C. Ting, 14 th International Conference on High-Energy Physics, Vienna (1968).

5. V.A. Sidorov, 4th International Symposium on Electron and Photon Interactions at High Energies, Liverpool (1969).

6. S. Devons, C. Sabat, P. Nemethy, E. Capua, A. Lanzara, Phys. Rev., 184, 1356 (1969).

7. Yu. S. Surovtsev, F.G. Tkebuchava. Coobshcheniya OIYaI (JINR Communications), P2-4561 and P2 4524. Dubna 1969.

8. A.V. Tarasov, L.G. Tkachev. JINR Preprint, P2-4970, Dubna 1970.

9. V.S. Roganov, Publication submitted to JINR, BI-9-4707, Dubna, 1969.

10. K. Satta, K. Suga. Nuovo Cimento, ii, 600 (1959).

11. V.I. Rykalin, T.G. Kmita, I.V. Ryzhikov, I.N. Novoselova. JINR Preprint, 2466, Dubna 1965.

12. V.M. Kut'in, V.I. Petrukhin, V.M. Tsupko-Sitnikov. JINR Preprint, 13-2677, Dubna 1966.

13. A. Tyapkin. Proceedings of the International Conference on Instrumentation N.Y.-Lond. Sept. (1960).

14. A.F. Dunaitsev, V.I. Petrukhin, Yu. D. Prokoshkin, V.I. Rykalin. PTE (Instrum. Exper. Tech.), 2, 114 (1965).

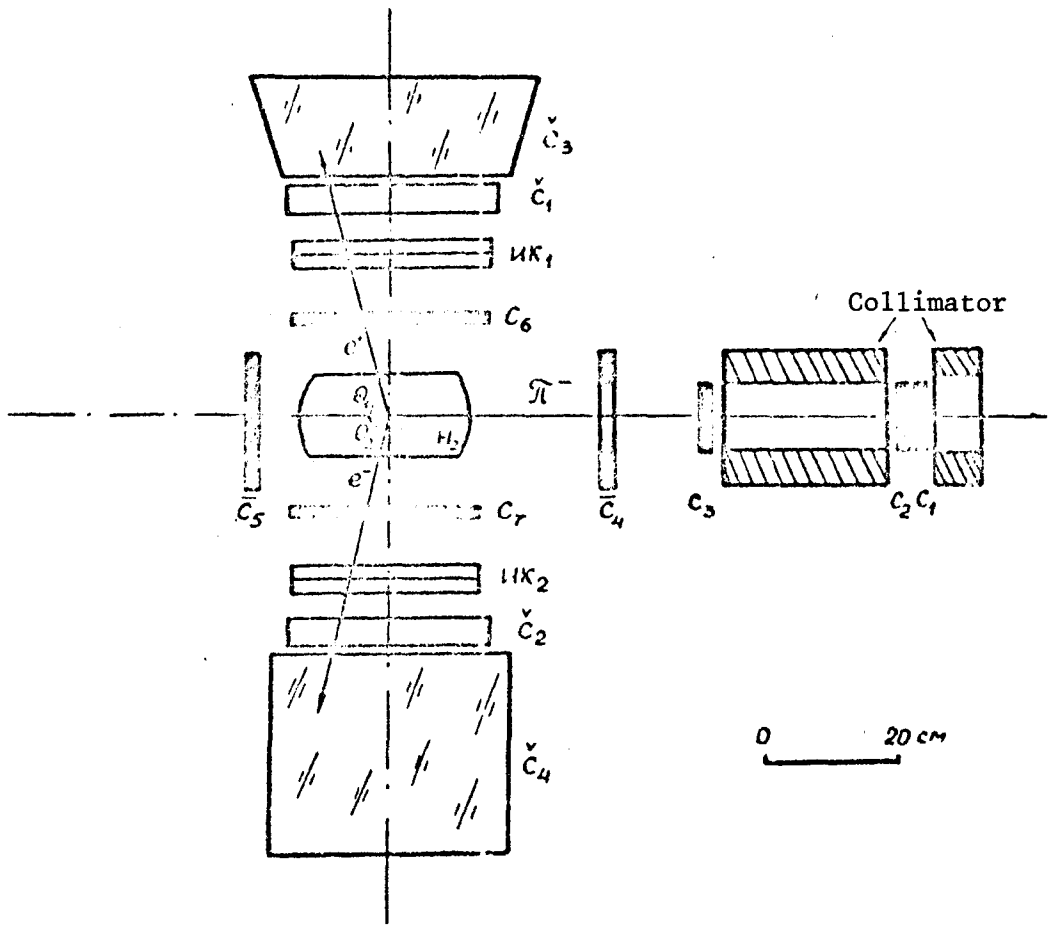

Figure 1

Diagram of experimental device. π^- beam incident on hydrogen target H_2, C_1 - C_7 - scintillation counters, $\check{C}_1$ and $\check{C}_2$ - threshold Čerenkov counters, $\check{C}_3$ and $\check{C}_4$ - Čerenkov spectrometers, IK, and IK_2 - spark chambers.

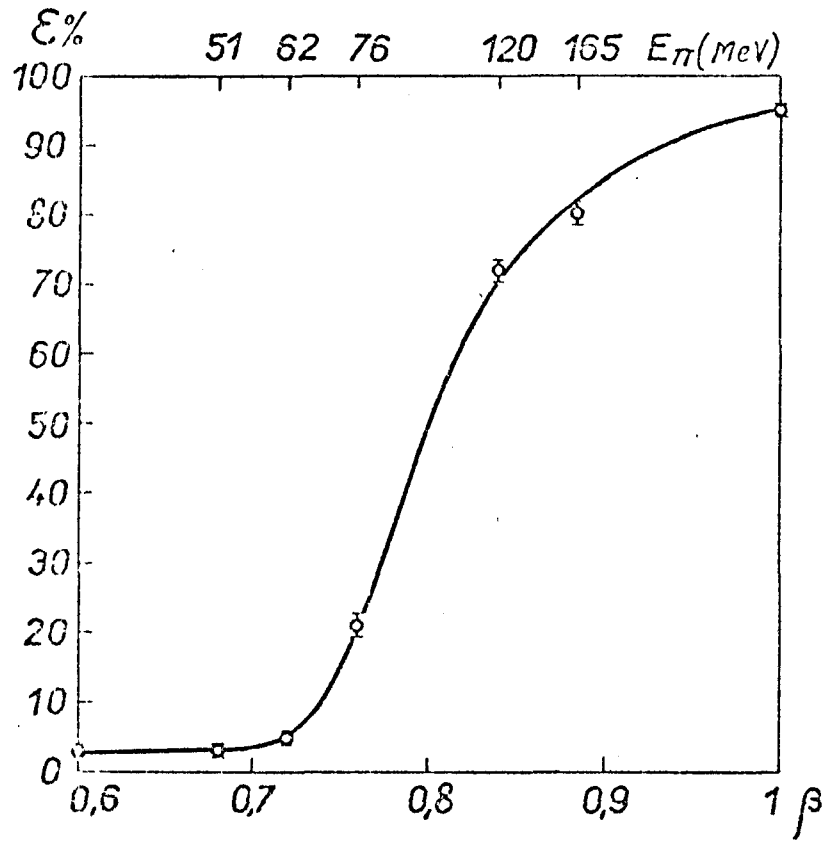

Figure 2

Dependence of Čerenkov counter's efficiency ε on the velocity β and kinetic energy E_{π} of the π mesons. The curve is drawn by hand from the experimental data.

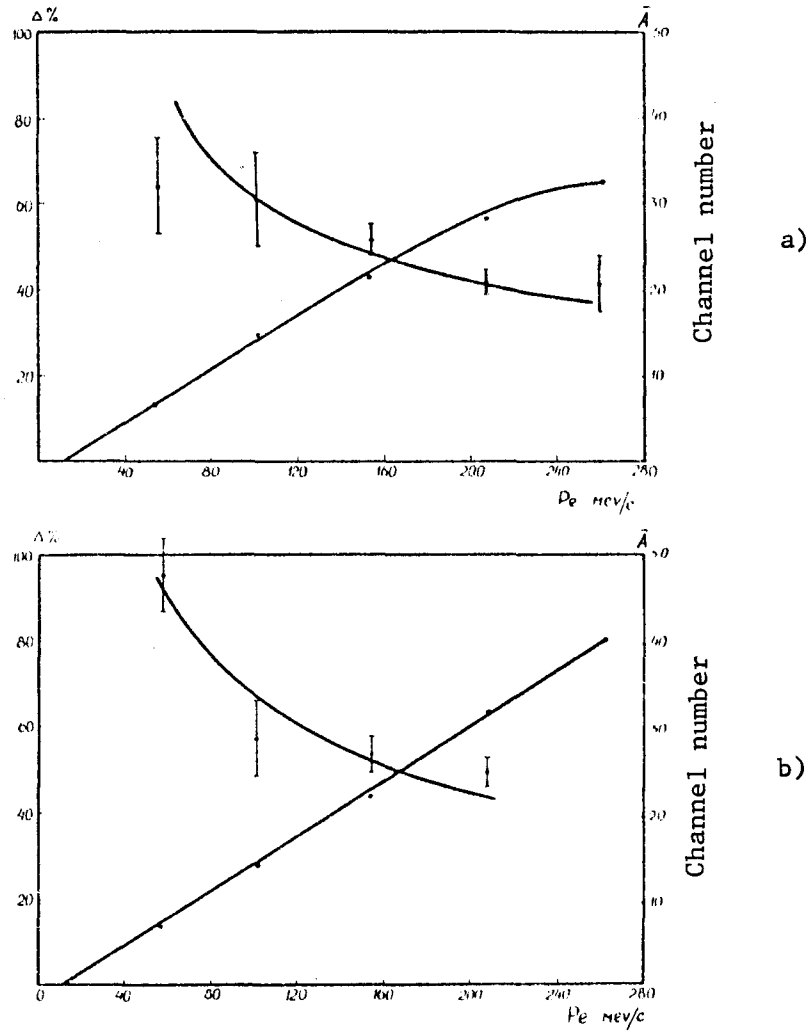

Figure 3

Dependence of the mean height $\bar{A}$ of pulses from the Čerenkov spectrometer and its resolution Δ (width at half-height) on the electron energy at the input of the side telescope, a) for $\check{C}_3$, b) for $\check{C}_4$. Electron energy losses in the side telescope's scintillation and Čerenkov counters total 12 MeV.

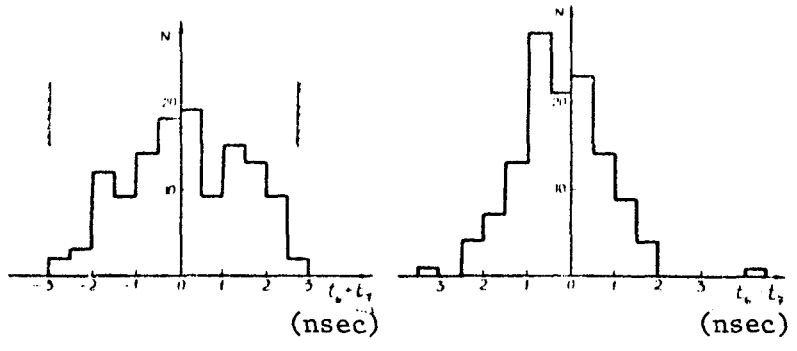

Figure 4 a

Distributions of candidate events in terms of the total number of time shifts of signals from the side scintillation counters C_6 and C_7 in relation to reference counter C_3 $(t_6 + t_7)$ and in terms of the time shifts between the signals from counters C_6 and C_7 $(t_6 - t_7)$;

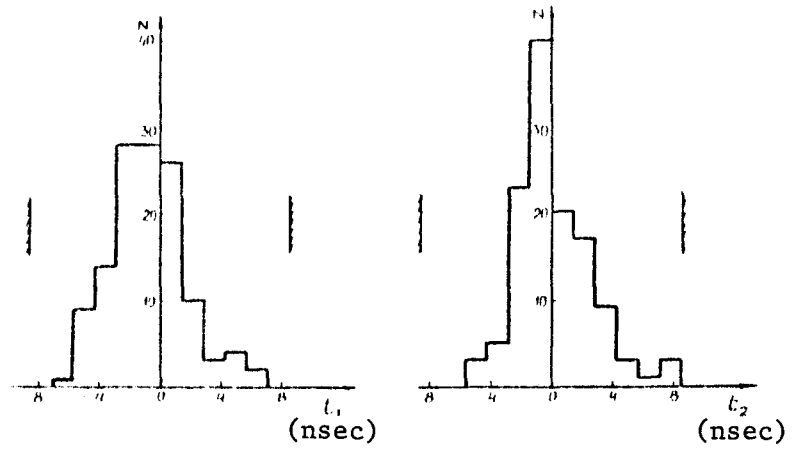

Figure 4 b

Distributions of candidates in terms of the time shifts of signals from spectrometers $\check{C}_3$ (t_1) and $\check{C}_4$ (t_2) in relation to reference counter C_3. The average of the corresponding values obtained from the calibrations is taken as zero. The limits within which candidates were selected are shown.

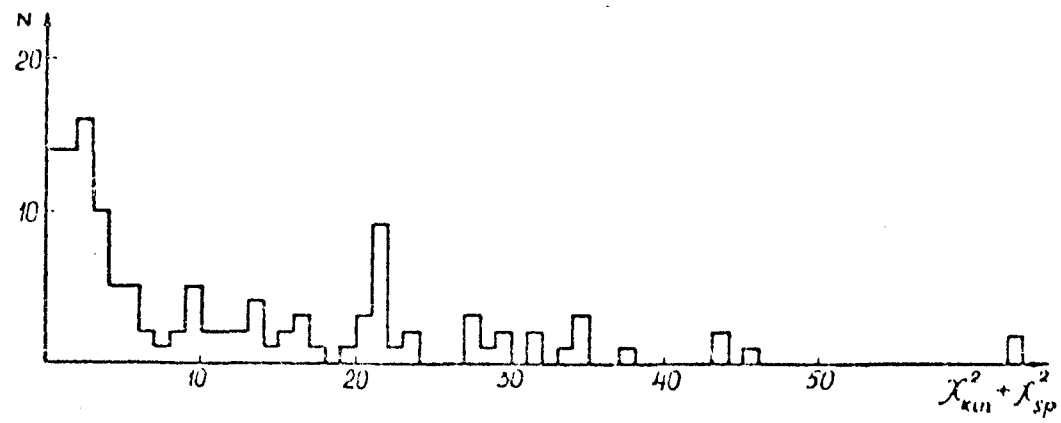

a)

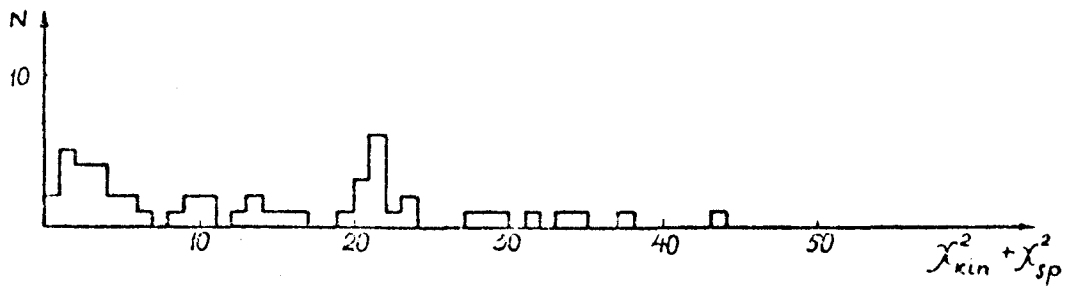

b)

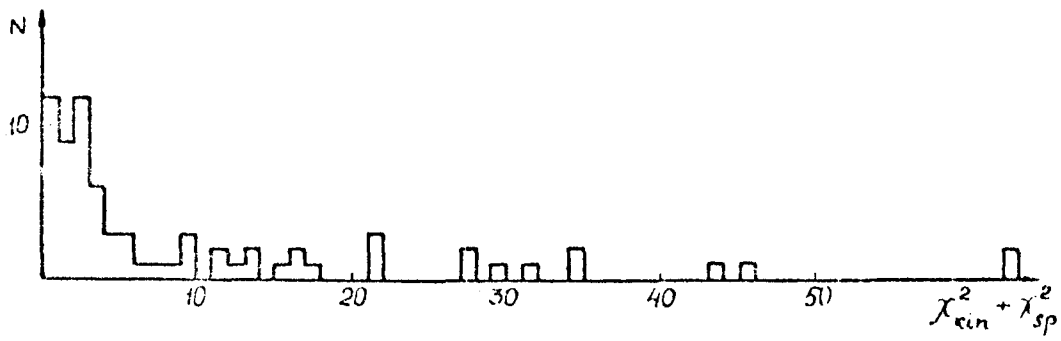

c)

Figure 5

Distribution of candidate events in terms of the value $X^2_{kin} + X^2_{sp}$

a) for all candidates (125 events);

b & c) for candidates split up according to the ionization losses in counters C_6 and C_7;

b) 52 events when A_6 or $A_7 > A_o = 1{,}6A$ prob.

c) 73 events when A_6 and $A_7 < A_o$.

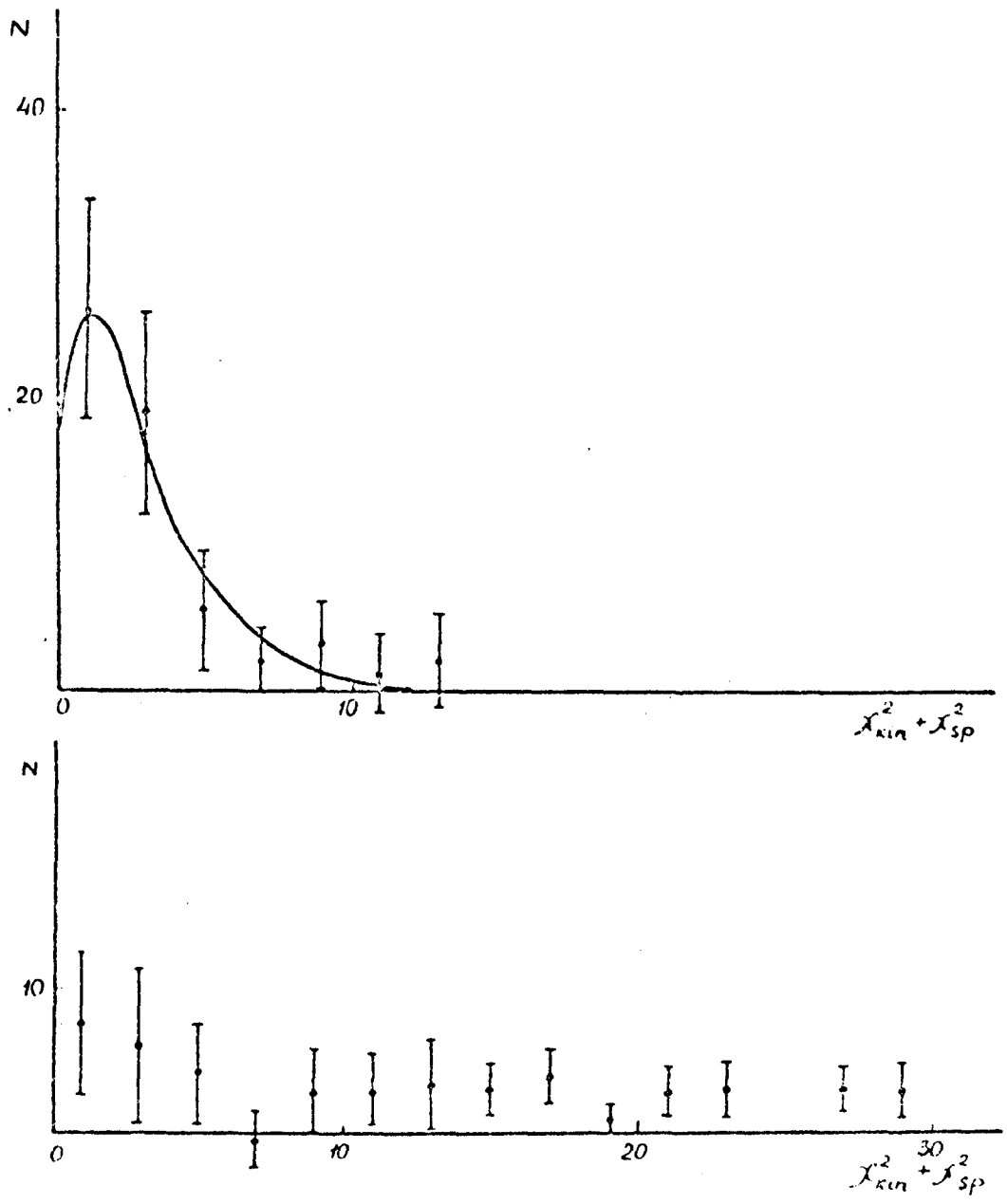

Figure 6

Distributions in terms of $X^2_{kin} + X^2_{sp}$ of reaction (1) events (a) and background events (b) split up by means of relationship (2). The curve corresponds to the X^2 distribution with three degrees of freedom.

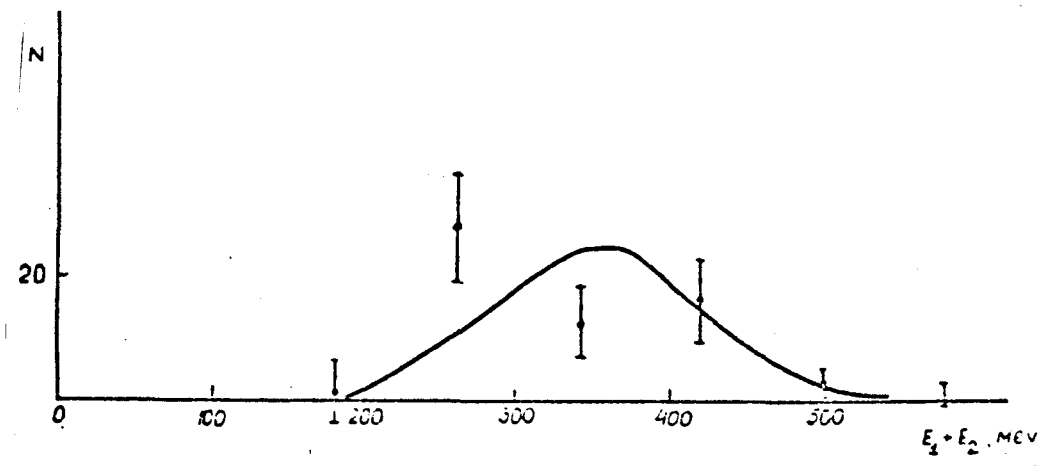

a)

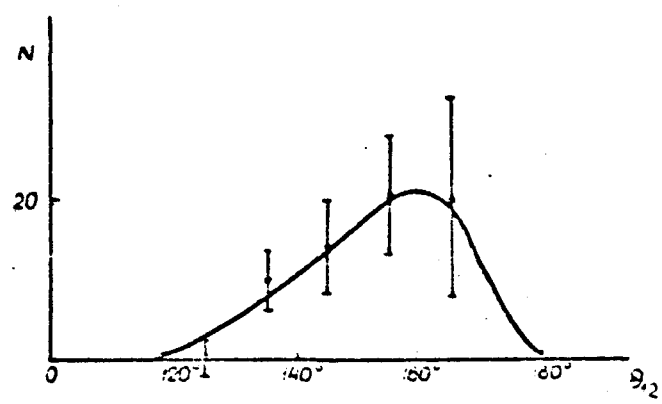

b)

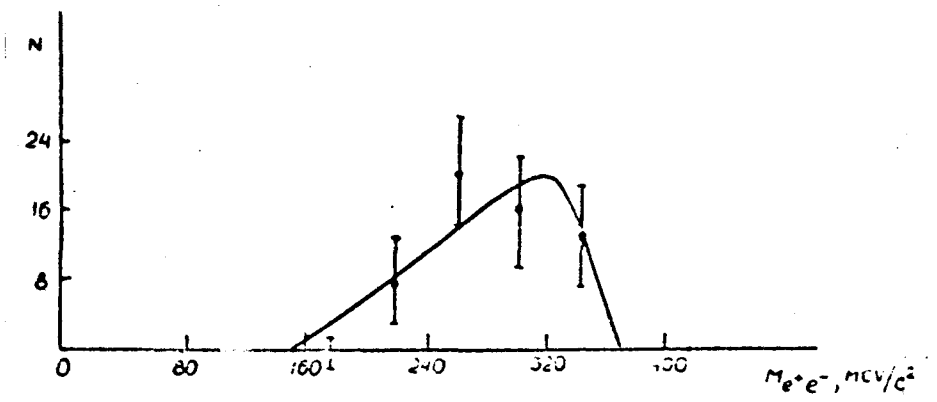

c)

Figure 7

Distribution of reaction (1) events in terms of the total electron and positron energy (a), in terms of the angle between them θ_{12} (b) and in terms of the effective mass of the $M_{e^+e^-}$ pair (c). The solid curves are based on a statistical model.